IOP Publishing Journal of Geophysics and Engineering
J. Geophys. Eng. **10** (2013) 035001 (10pp) doi:10.1088/1742-2132/10/3/035001

Investigation of the subsurface geometry of fissure-ridge travertine with GPR, Pamukkale, western Turkey

Cahit Çağlar Yalçiner

Department of Geophysics, Çanakkale Onsekiz Mart University, Çanakkale, Turkey

E-mail: yalciner@comu.edu.tr

Received 1 March 2013
Accepted for publication 10 April 2013
Published 3 May 2013
Online at stacks.iop.org/JGE/10/035001

Abstract

Cracks in the upper crust are the result of either local or regional tectonic stress. Such structural elements are conduits for fluids in the crust. In Pamukkale, hot water which is rich in calcium carbonate emerges from fissures. The hot water issuing from the fissures precipitates travertine both in the fissures and on the surface. As a result, a ridge, which is called fissure-ridge travertine, forms along the central fissure. Fissure-ridge travertines are lens-shaped at the surface. Since fissure-ridge travertines are of great tectonic significance, their surface characteristics have been studied in detail. However, the subsurface geometry of travertine ridges is not well known. GPR was used to examine the subsurface geometry of fissure-ridge travertine and the central fissure. GPR profiles were combined across the ridge to produce a three-dimensional (3D) subsurface image of the travertine mass. The 3D image showed that the thickness and width of the travertine mass are at a maximum near the centre of the ridge and they both decrease asymmetrically towards the ends. Perpendicular GPR slices across the central fissure showed that the thickness of the vertically banded fissure-travertine increases with depth. 3D modelling suggests that the lateral propagation of the central fissure is asymmetric.

Keywords: ground penetrating radar, fissure-ridge travertine, Pamukkale

(Some figures may appear in colour only in the online journal)

1. Introduction

Travertine is a hard, compact limestone deposited from solution by spring water (Wyatt 1986). There is a worldwide association of travertine deposits with tectonically and seismically active zones, because fracturing plays a key role in the transport of hydrothermal fluids (e.g., Sibson *et al* 1975, Barnes *et al* 1978). Fissure-ridge travertines (a morphological type of travertine defined by Chafetz and Folk (1984)) are deposited by hot water issuing from springs cutting the underlying bedrocks. A travertine ridge contains a central fissure along its crest. Water rises to the surface via this nearly vertical fissure. A typical fissure-ridge travertine (figure 1(*a*)) comprises flanking bedded travertines dipping away from the fissure, and a nearly vertical central fissure filled by fissure travertine. Bedded travertines form as a result of flow away from the source fissure at the surface. Thus, ridges with sloping sides gradually develop adjacent to fissures (Jones 1925). Fissure travertine forms while water is rising within the fissure. Such travertines are generally banded and sub-parallel to fissure walls (Altunel 1994). Fissure travertines are compact and hard, whereas bedded travertines are hard but porous.

The Pamukkale area in western Turkey provides a unique example of the relationship between travertine deposition and tectonic structures (e.g., Altunel and Hancock 1993a, 1993b, Altunel 1994, Hancock *et al* 1999). The Pamukkale travertines are located in the northern side of the Denizli basin (figure 1(*b*)), situated close to the eastern limit of the Aegean extensional province, oriented approximately NNE–SSW. The travertine area is bounded to the northeast by the

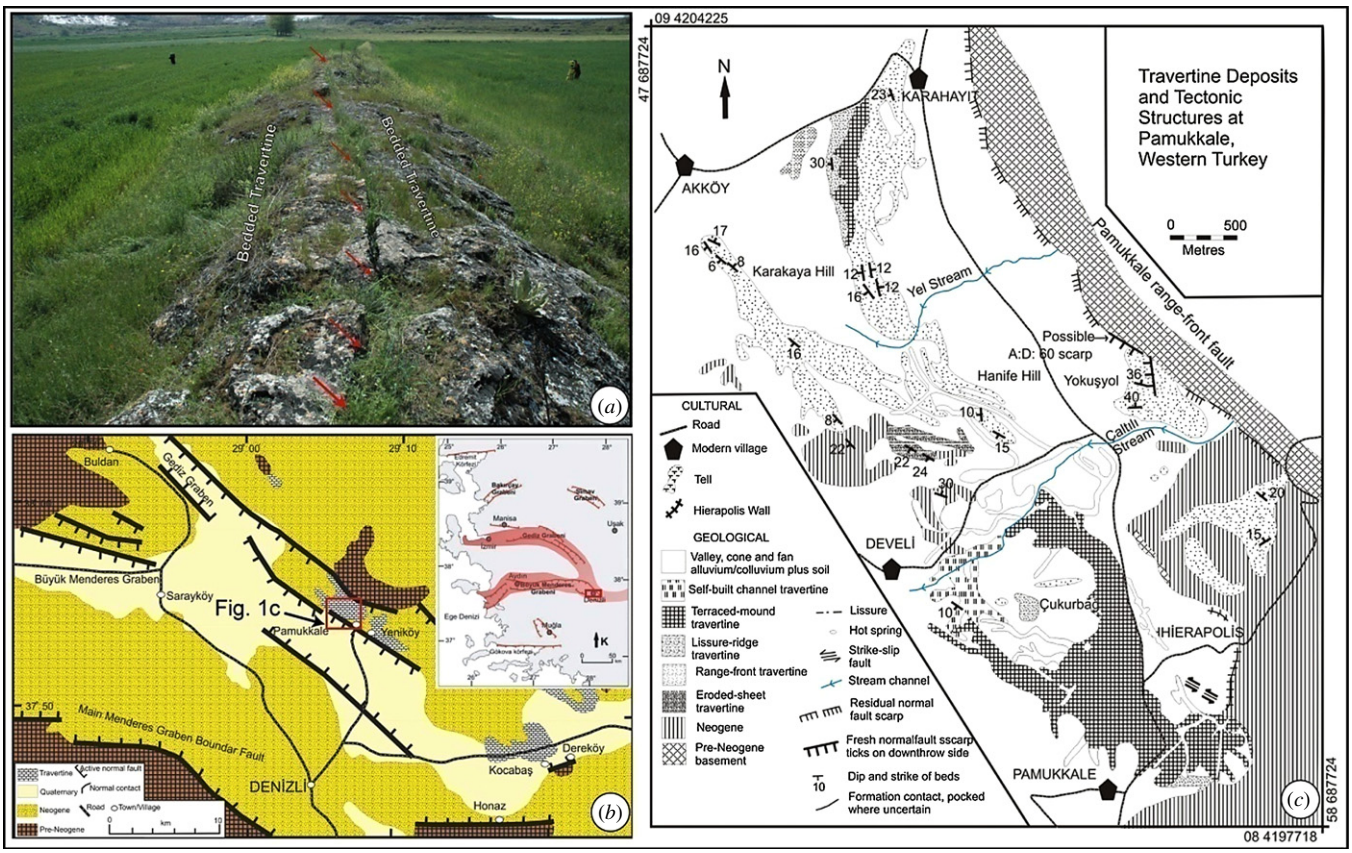

Figure 1. (*a*) A typical fissure-ridge travertine (red arrows indicate central fissure). (*b*) Simplified geological map of the Denizli basin with major active tectonic structures. (*c*) Detailed geological map of the Pamukkale travertine area.

Pamukkale range-front (figure 1(*c*)), a topographic feature expressing a normal fault with a down-throw of at least 450 m into the Denizli basin (Altunel and Hancock 1993a, 1993b). As figure 1(*b*) shows, the southwestern side of the travertine area is also bounded by a normal fault down-throwing southwest (Saroglu *et al* 1992).

Fissure-ridge travertines are located in the hanging wall of the Pamukkale range-front fault in a roughly NW–SE-trending zone, which Altunel (1994) termed the Pamukkale fissure zone. The long axes of the travertine ridges extend in various directions throughout the Pamukkale Plateau, but mainly trend NNW–SSE; that is, sub-parallel to the Pamukkale range-front fault (figure 1(*b*)). The studied ridge is located in the Çukurbağ area (about 1 km north of Pamukkale village), where fissure ridges extend in both E–W and NW–SE directions (figure 1(*c*)). The trend of the studied ridge is NW–SE.

According to Altunel (1994), fissure-ridge travertines are of great tectonic significance because the architecture and layout of masses might reflect some aspects of tectonic structures cutting the upper crust. The surface characteristics of fissure-ridge travertines have been investigated for at least the last two decades in order to understand fracture propagation in the upper crust (e.g., Altunel and Hancock 1993a, 1993b, 1996, Altunel 1994, Cakir 1999). Interpretations were mainly based on the surface characteristics of travertine ridges. Quarries in travertine ridges provide good opportunities to investigate a ridge in detail, but they are very limited. Recently, the development of ground penetrating radar (GPR) antennas provided the most powerful nondestructive geophysical prospecting method to investigate shallow subsurface features, and can be used to identify the detailed subsurface geometry of travertine ridges.

The purpose of this paper is to investigate the subsurface geometry and internal structures of a fissure-ridge travertine in Pamukkale, western Turkey, using GPR. The ridge was scanned in detail using GPR, and its subsurface geometry was modelled in three dimensions (3D). Illustration of the subsurface layout of fissure-ridge travertine would contribute to understanding the evolution of the ridge along the fissure; and further the understanding of near-surface fracture mechanics in the upper crust.

2. GPR methodology

GPR is a near-surface geophysical technique that facilitates the discovery and mapping of buried features in ways not possible using traditional field-survey methods (Conyers 2006). GPR data acquisition involves the transmission of high-frequency (10 MHz–2.3 GHz) radar pulses from a transmitter antenna into the ground. The radar waves travel at the speed of light (0.3 m ns^{-1}) in air, but slow significantly when penetrating the ground. At each interface where its speed changes, some of those waves are reflected back to the surface. The greater the velocity change, the higher the amplitude of the reflected radar waves. The elapsed time between when radar waves are transmitted; reflected from buried materials or sediment,

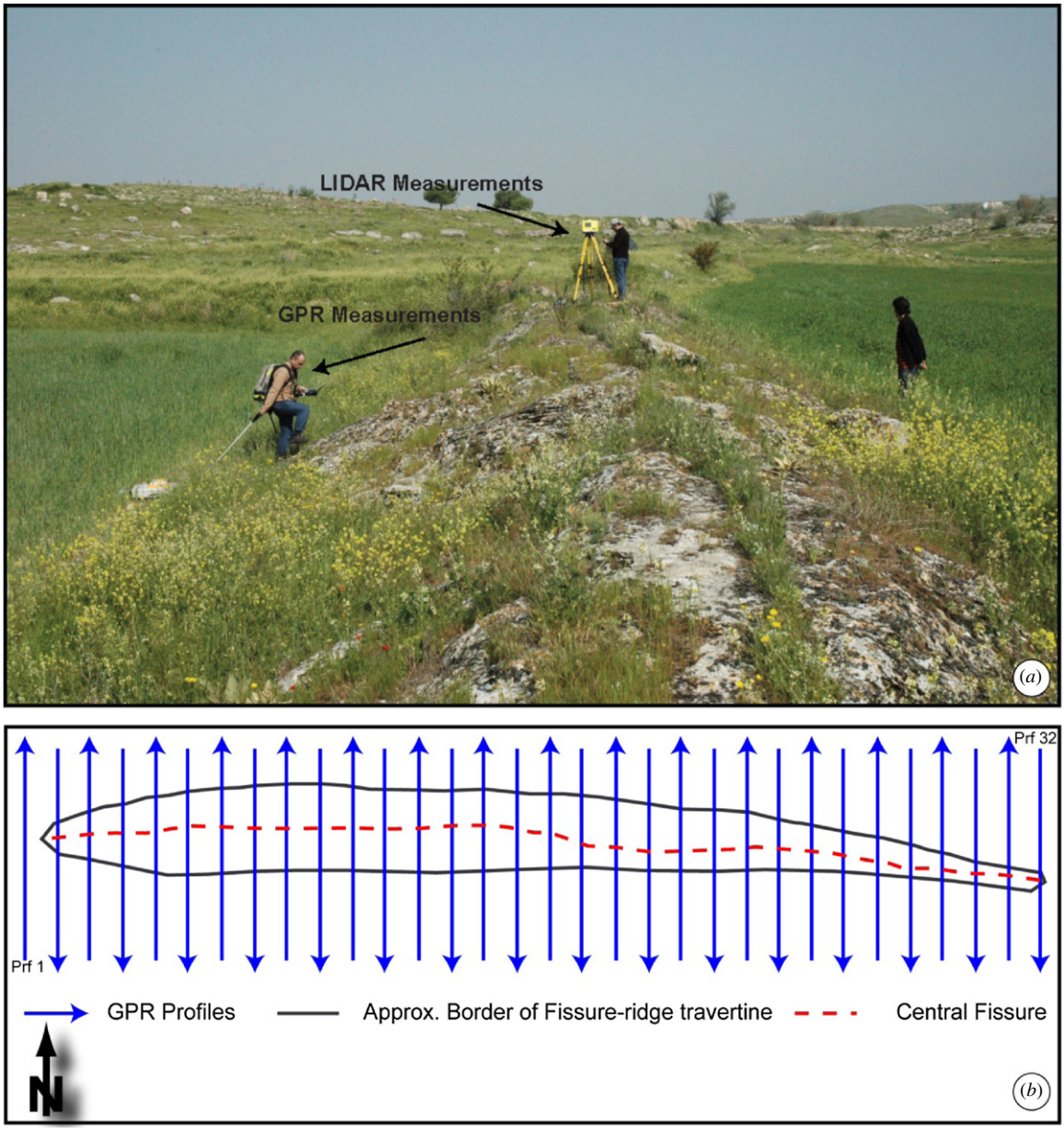

Figure 2. (*a*) View of a fissure-ridge travertine (view towards west). (*b*) Plan view of the studied fissure ridge obtained with LIDAR. GPR profiles were taken perpendicular to the long axis of the ridge.

and soil changes in the ground; and then received back at the surface is then measured for depth scale. The system records all waves (air waves, reflected waves, and diffraction waves) as traces. Many hundreds or even thousands of traces are measured and recorded, as antennas are moved along transects within a constant trace interval (1–50 cm), which are then used to create two-dimensional profiles. When two-dimensional profiles are collected parallel to each other in a grid manner, 3D maps can be constructed, making the GPR method one of the most precise tools for mapping buried features (Conyers 2006).

When the GPR equipment is used for 3D applications, a grid search should be employed, with equidistant spacing (3 m for 250 MHz) between contiguous transect lines. The GPR system can then be pulled over each of the grid transect lines to collect data. With the antenna positioned at the bottom of the shielded system, in close proximity to the ground surface, short-duration electromagnetic (EM) pulses are emitted downward into the ground from the bottom of the shielded antenna. The most common means of displaying 3D radar data is in 'time slice' maps (Conyers 2004). Time slices are the easiest and most rapid way to generate a synthetic plan of anomaly patterns, especially for large areas. On the other hand, for smaller areas, the 3D cubes presentation technique gives a more complete understanding of subsurface features, with clear views, and slices parallel to the axes or along arbitrary directions (Leucci and Negri 2006).

2.1. Data acquisition

The geophysical instrument used for this study was a Mala RAMAC ProEX GPR unit with 250 MHz shielded antenna.

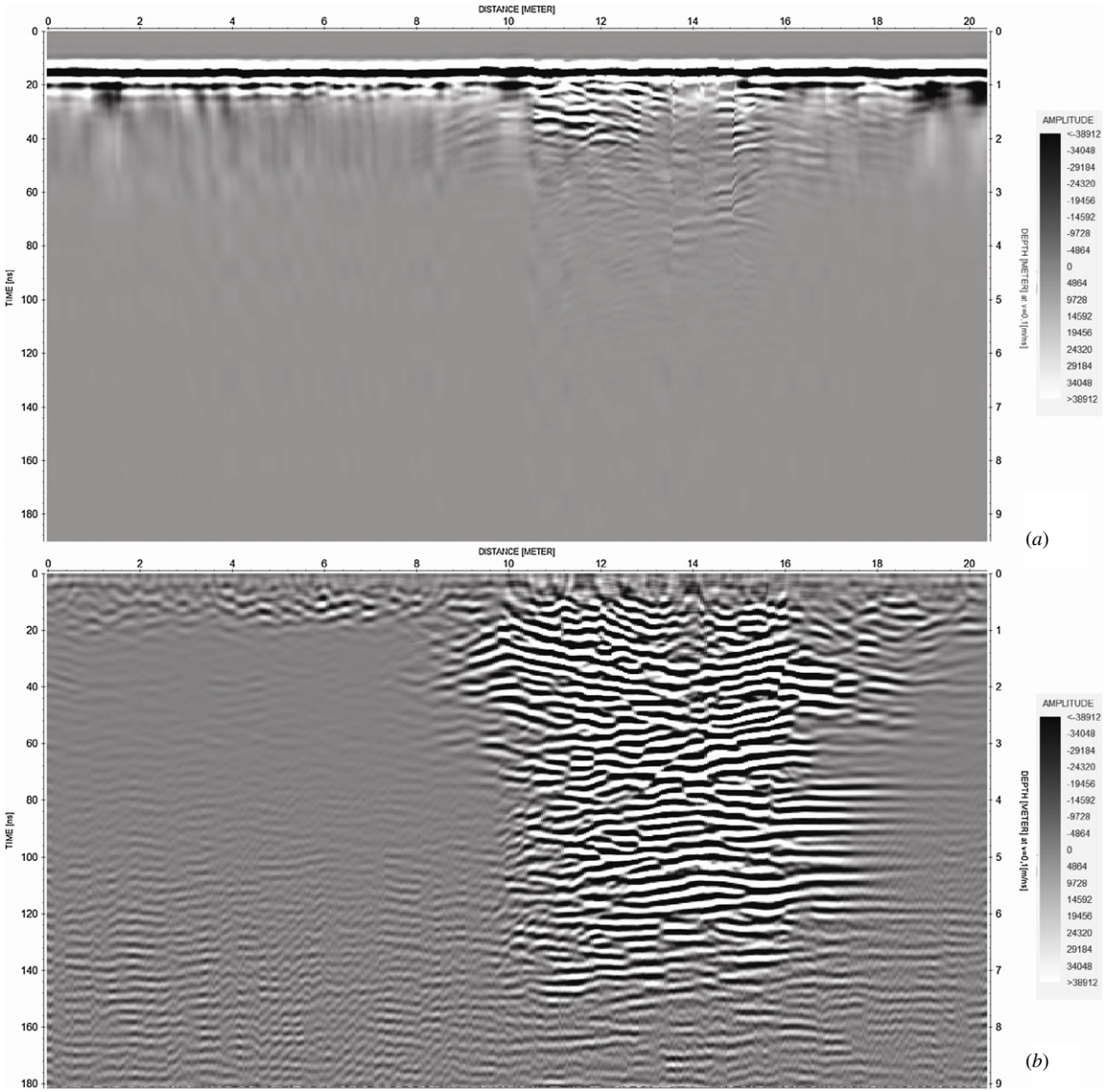

Figure 3. An example of a GPR profile (profile 23) on the studied fissure-ridge. (*a*) Raw data. (*b*) Processed data (including all processing steps except topographic correction).

Table 1. Acquisition parameters of the GPR survey.

Antenna Freq.	250 MHz
Trace interval	0.05 m
Samples	512
Sampling freq.	2607 MHz
Time window	196 ns
Profile intervals	3 m

The antenna was oriented in the normal position (true orientation) on the ground (figure 2(*a*)). In 2D GPR studies, the best subsurface images are obtained by cutting the target perpendicularly. Thus, the profile was taken in a rectangular area and perpendicular to the central fissure of the fissure-ridge travertine (figure 2(*b*)). Large topographic variation along the profile affects the penetration of the EM signals, but topographic correction was applied, as mentioned in the processing steps. The topographic data used for the topographic correction, and locations of the profiles, were determined by high-sensitivity LIDAR (laser imaging detection and ranging) equipment (figure 2(*a*)). In the present study, both 3D time slices and 3D cube visualization techniques were used. The acquisition parameters used in GPR surveys are given in table 1.

2.2. Data processing

Reflex W software was used to improve the quality of the original data with respect to the signal to noise ratio, to reduce unwanted clutter, and to facilitate better interpretation (Sandmeier 2003). Figure 3 shows an example of processed radar data. The main processing steps are summarized in table 2.

The EM wave velocity was estimated in order to define the depth of anomalies. The characteristic hyperbolic shape of a reflection from a point source (diffraction hyperbola) is the easiest way to determine EM wave velocity from profiles

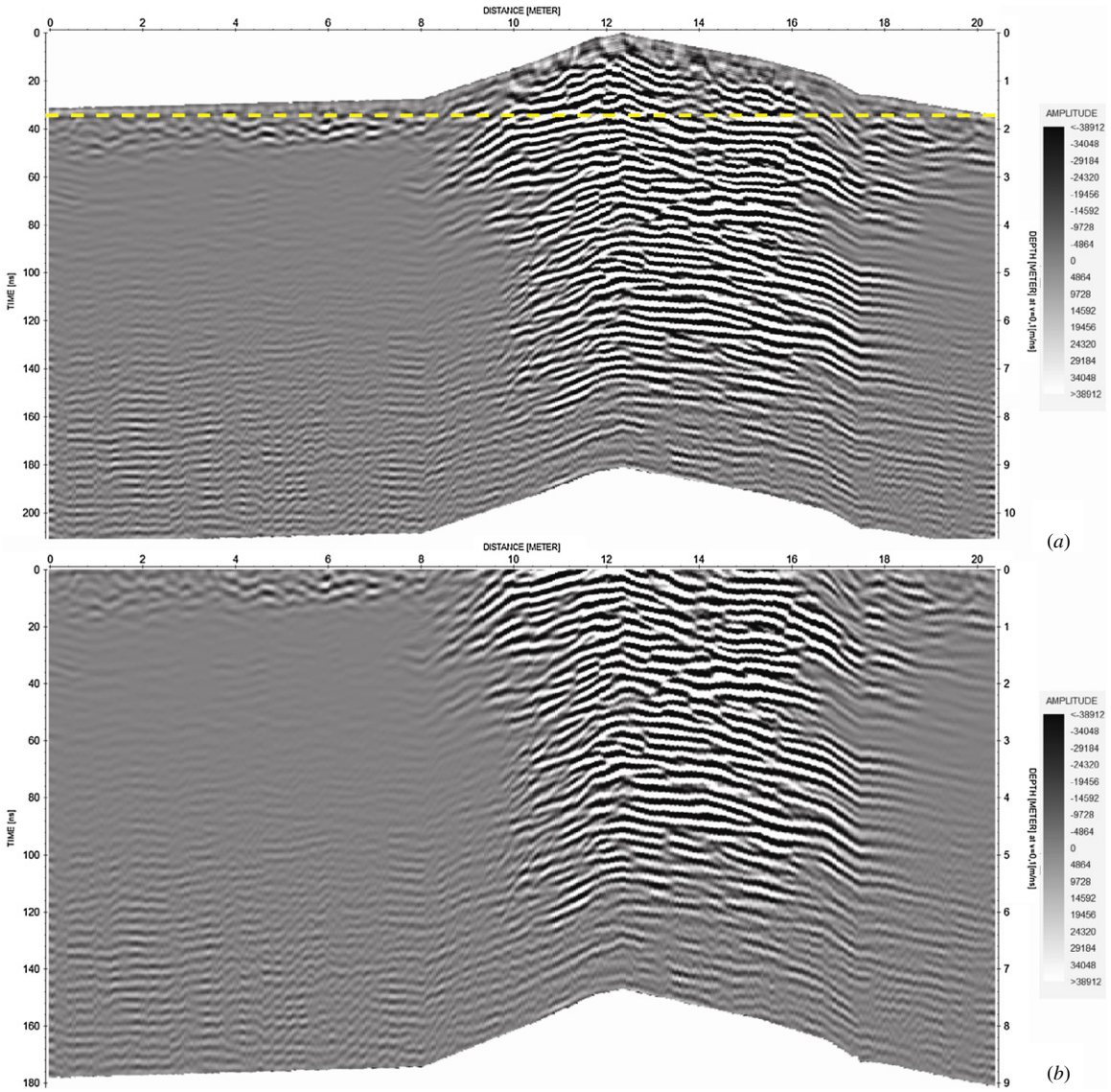

Figure 4. (*a*) GPR profile (profile 23) after the application of topographic correction. Yellow dashed line represents the surface level. (*b*) Flat topography, ridge above the flat surface was removed.

Table 2. Filter processing steps and parameters of the GPR survey.

Filter name	Parameters
Time-zero correction	−9 ns
Running average filter	4 ns
Energy decay	0.512
Subtracting average	31 trace −6 to 196 ns
Band-pass filter	100–200–300–400 MHz
Velocity analysis	0.1 m ns^{-1}
Diffraction stack migration	31 trace/0.1 m ns^{-1}/0–196 ns/$\varepsilon_r = 9$
Topographic correction	Different for each profile

acquired in continuous mode. A result indicated a velocity of 0.1 m ns^{-1}, which gives an average relative dielectric constant ε_r equal to 9.

The final stage of processing GPR data is wave migration, which refocuses collected time responses so that the images more closely resemble the physical target dimensions (Song *et al* 2006, Kadioglu and Ulugergerli 2012). Migration is generally used to improve section resolution, and to develop more spatially realistic images of the subsurface, but is, arguably, the most controversial of the GPR processing techniques (Cassidy 2009). Moran *et al* (2000) adapted the Kirchhoff (diffraction stack) integral of Schneider (1978) with the inclusion of a half-space interfacial dipole radiation pattern, and applied this modified migration equation to both synthetic data and glacier data. Their modified GPR formulation is given by

$$U(r) = \frac{1}{2\pi} \int_{z'=0} \frac{E^{\alpha}(\theta, \phi, \varepsilon_r)}{R^{\beta} \upsilon} \frac{\partial U(r'_0, t_0)}{\partial t} \mathrm{d}a'_0,$$

where U is the migration depth image, and $U(r'_0, t_0)$ is the surface wavefield observation. Primed parameters z', r', and a' give spatial dimensions relative to an array's coordinate origin, R is the subsurface diffraction point relative to a surface observation, r is the integral evaluation point relative to the array's coordinate origin, υ is the propagation speed in soil, and $E(\theta, \phi, \varepsilon_r)$ is the range normalized electric field

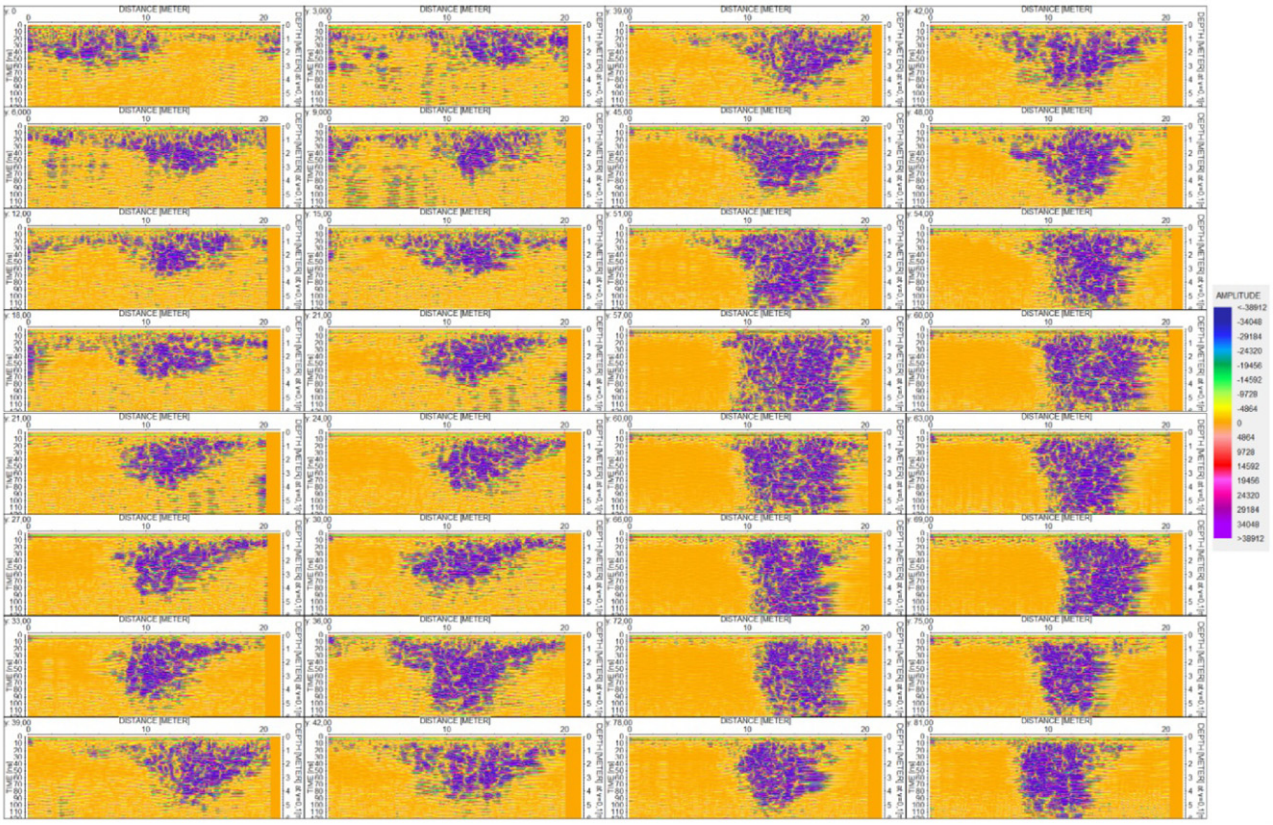

Figure 5. 2D views of all GPR profiles (32 profiles).

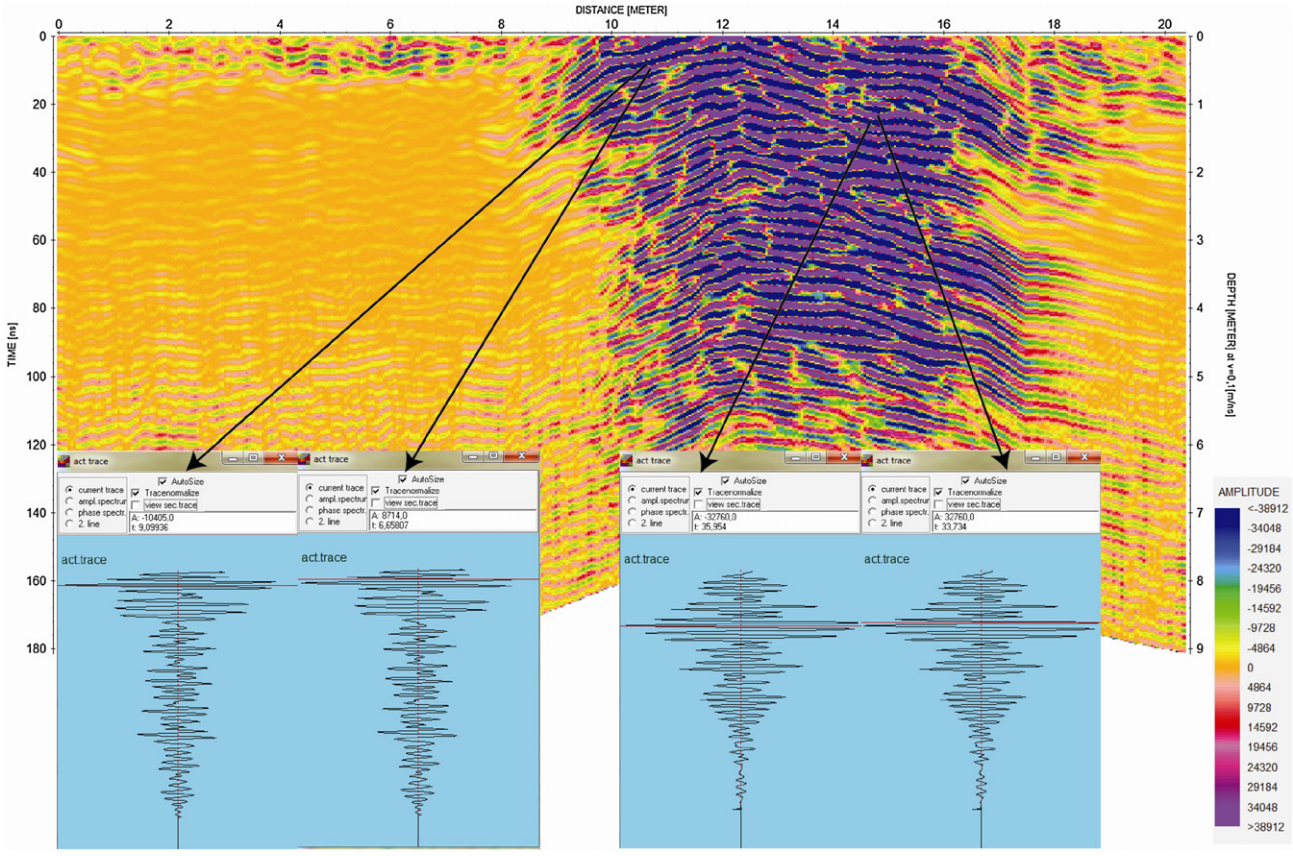

Figure 6. Amplitude measurements on the anomaly of travertines (compact and porous). Amplitudes change between −32.760 and 32.760 near the centre of the travertine (compact fissure travertine). Amplitudes change between −10.405 and 8.714 near the border of travertine (porous bedded travertine).

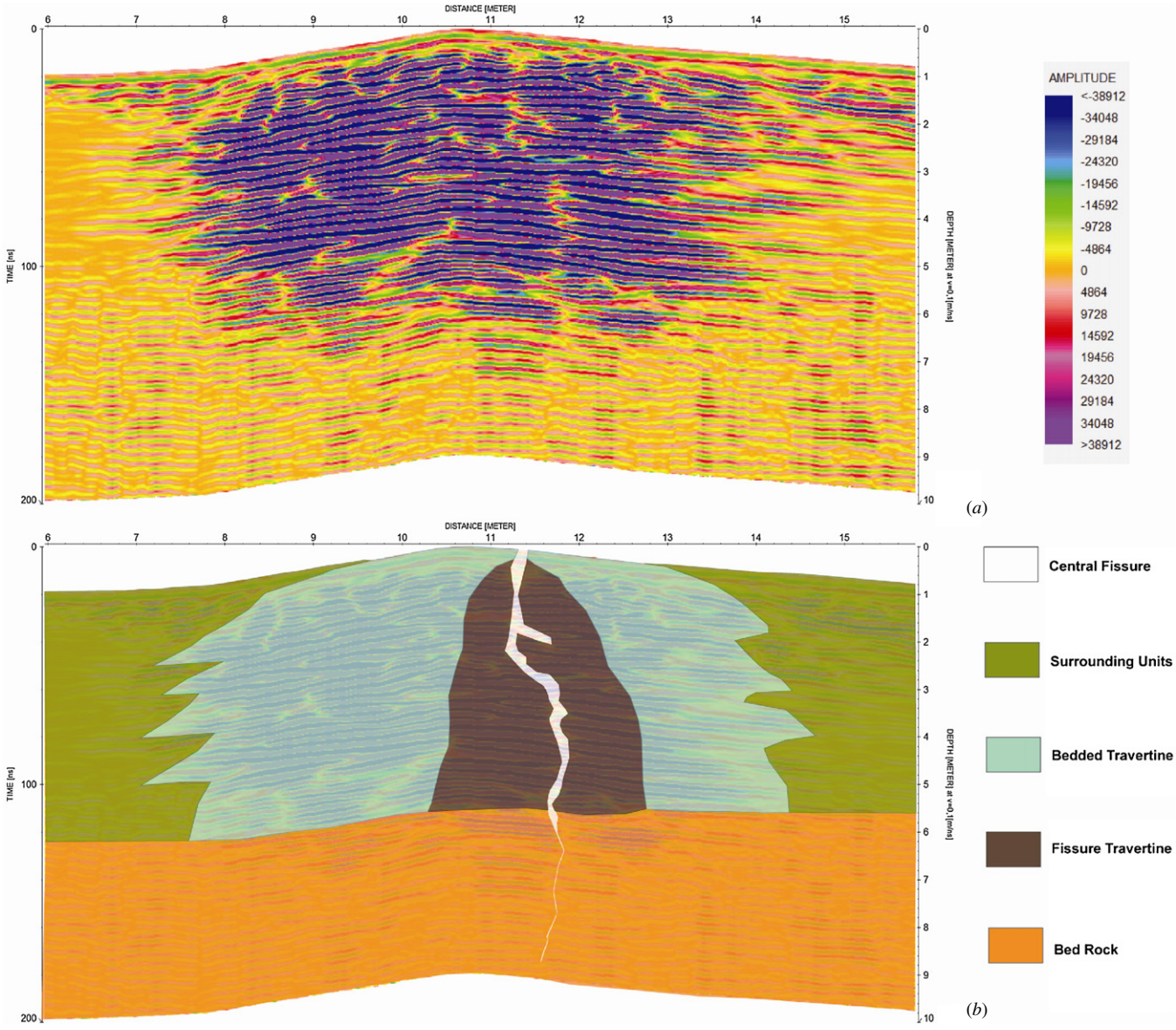

Figure 7. Interpreted GPR profile (profile 23). (*a*) Processed GPR data. (*b*) Modelled GPR data.

dipole radiation pattern. The exponents α and β are treated as processing parameters to be determined by systematic trial-and-error variation.

In this work, the diffraction-stack method was applied to each profile separately via the above equation, which is used widely in seismic migration (French 1974). First, the EM velocity of the anomalous zone was determined (0.1 m ns^{-1}). Then the diffraction-stack method was applied to each whole profile (figure 3(*b*)) with the parameters listed in table 2. After processing the raw data, topographic correction was applied to each profile with different correction parameters (figure 4(*a*)).

Data sets which need topographic corrections must migrate with real topographic geometry for the most reliable results. In principle, it is possible to migrate by considering the real geometry, but it could be rather computational complex. For these reasons in this study I took into account the tolerances and topographic correction was applied after the migration processing steps.

In 2D profiles, high-amplitude zones on traceable flat continuous reflectors in the processed data can reflect vertically and horizontally beneath the surface. Thus, these anomalous zones require detailed observation to determine the exact position, size, and depth of the travertine. 3D data sets were obtained by interpolation of processed 2D profiles without any extra processing except flattening the topography of the 2D profiles (figure 4(*b*)), the results may be presented by several different methods (time slice, iso-amplitude surface, etc).

2.3. Data presentation

The collected GPR data was processed via suitable filters, which produced results and images that may be understood and applied in other disciplines (archaeology, geology etc). GPR data of fissure-ridge travertine in Pamukkale is presented in 2D to show the ridge in profile, and in 3D to show the subsurface geometry of the ridge.

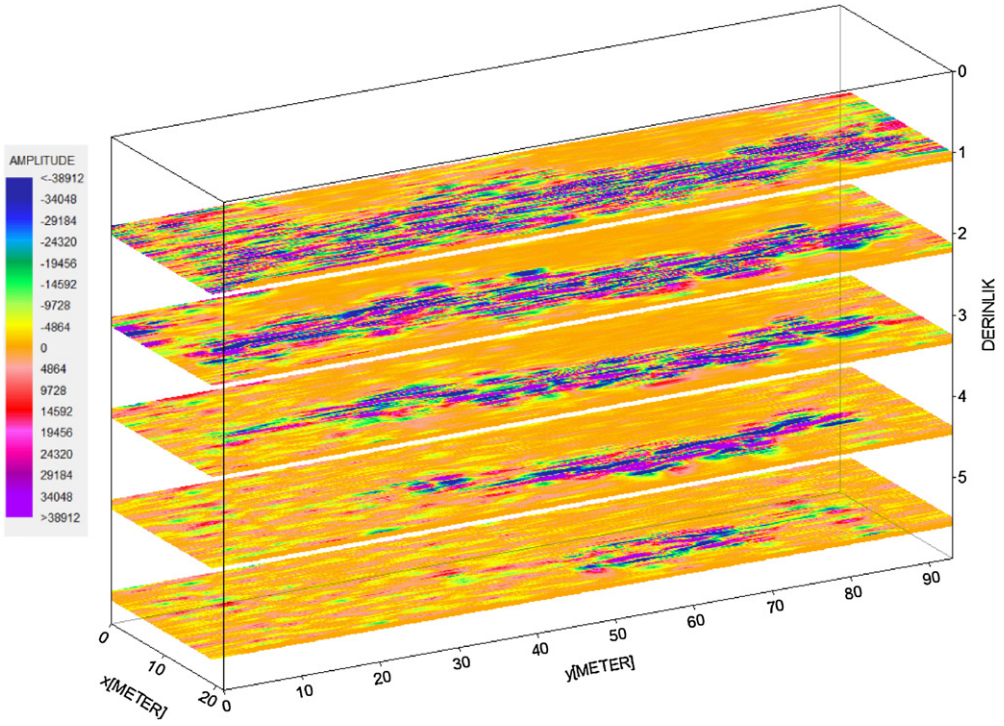

Figure 8. 3D time slices for different depths.

2.3.1. 2D data presentation. Figure 5 shows all GPR profiles across the E–W-trending fissure-ridge travertine. It is clear that there is a strong anomaly in all profiles, resulting from the different dielectric constants between the travertine and surrounding units. Detailed examination of the travertine anomaly showed that amplitude changes are much greater in the central part ('−32.760/32.760') compared with those near the border of the anomaly ('−10.405/8.714') (figure 6). Previous GPR studies on natural stones showed strong reflectors (high energy) associated with prominent fractures or compact stone blocks (Porsani *et al* 2006). Considering their physical properties, fissure travertines are much more compact than bedded travertines. Thus, the strong reflectors (higher energy) are regarded as fissure travertines and weak reflectors (lower energy) are regarded as bedded travertines in this study. Based on amplitude changes, the limits of the fissure travertines and bedded travertines were determined with the amplitude threshold in the amplitude map (figure 7).

2.3.2. 3D data presentation. The generation of horizontal time-slices from GPR profiles provides visually useful maps of the plan distribution of reflection amplitudes within specific time intervals (Conyers 2004). This data representation (figure 8) plays an important role in GPR investigations, as it allows easier correlation of the most important reflections found within an area at the same depth, thus simplifying interpretation (Carrozzo *et al* 2003). However, it should be noted that the depth of time slices is approximate, due to possible changes in velocity with depth and lateral distance (Yalciner *et al* 2009).

The same data set is displayed via a 3D model, in order to more realistically show the shape of the travertine body beneath the surface (figure 9(*a*)). In order to reduce noise effects, changes in amplitude were limited between 5.000 and 30.000 for negative and positive amplitudes in the 3D modelling.

3D modelling of the GPR data (figure 9(*a*)) shows that the travertine has maximum thickness near the centre of the ridge, and that it thins asymmetrically towards both ends of the ridge (figure 9(*b*)).

3. Discussion and conclusions

During approximately the last two decades, GPR has become the most powerful nondestructive geophysical prospecting method in shallow geophysics. GPR provides significant advantages of high resolution and acquisition speed, and both 2D and 3D data recording capabilities. 3D interpretation of GPR data, and display methods such as time slices, have recently become popular in various forms of geological investigations (e.g., (Leckebusch 2003, Leucci and Negri 2006, Leckebusch *et al* 2008, Yalciner *et al* 2009). However, careful data processing and a good knowledge of both EM signalization and geology are required for reliable GPR results. The application of migration to field data showed that if migration is used with suitable parameters (such as EM velocity, bandwidth, start time and end time), it considerably reduces noise in profiles; and that anomalies become much clearer and assume their real shape.

Surface characteristics of the travertine ridges in the Pamukkale area were previously described in detail in several studies by Altunel and Hancock (1993a), (1993b), (1996) and Altunel (1994). However, their interpretations of subsurface travertine bodies were very limited. Central fissures

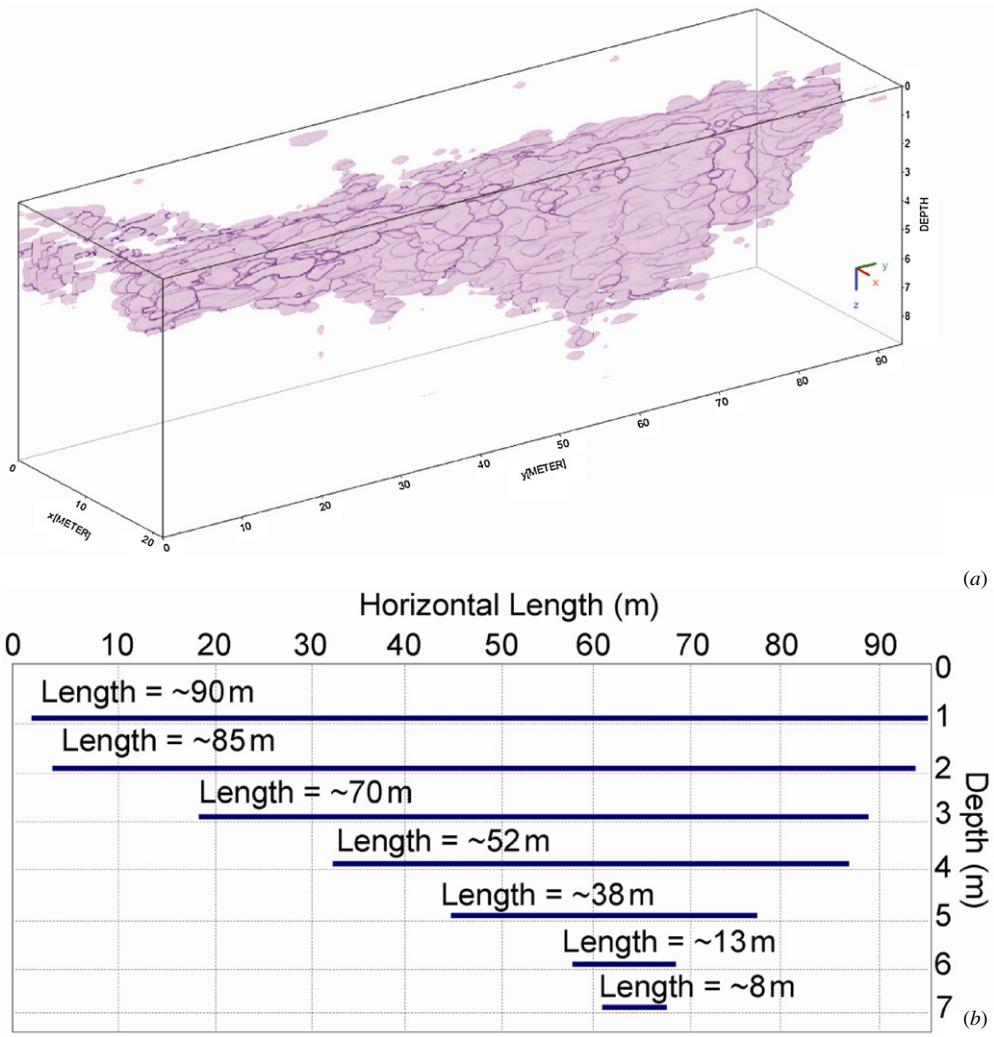

Figure 9. (*a*) Subsurface shape of the ridge obtained by 3D modelling. Note that the thickness of the travertine body decreases upwards asymmetrically. (*b*) Length of the ridge in various depths. Note that the length of the ridge is approximately 8 m about 7 m below the present surface level and it increases upwards.

are accompanied by ridges that approximately follow the crests of travertine ridges (figure 1(*a*)). Based on field observations, Altunel and Hancock (1996) suggested that the formation of a travertine ridge started near the centre of the ridge, and that the ridge prolongated along its long axis. 3D modelling of GPR profiles shows that the length of the ridge is short in depth and the length of the ridge increases upwards (figure 9(*b*)). The increasing length of the ridge upwards can be attributed to the development of the ridge. Figure 9(*b*) suggests that a ridge of about 8 m length started to form while the surface level was about 7 m lower than at present, and that the ridge prolongated asymmetrically over time. Thus, the maximum thickness of the travertine body is located where the ridge formation first initiated.

GPR profiles across the ridge showed different amplitude-changes (figure 6), which were attributed to the density of the travertine. It is suggested that lower and higher amplitude values represent bedded travertines (hard but porous) and fissure travertines (hard and compact), respectively (figure 7). Examination of GPR data across the ridge (2D data presentation) shows that the width of fissure travertines increases with depth (figure 7). Fissure ridges were also examined in profile where they were quarried in Turkey (Altunel 1994, Hancock *et al* 1999, Altunel and Hancock 1996, Mesci *et al* 2008). Based on limited field observations, Altunel and Hancock (1996) suggested that the width of fissure travertines (precipitated on walls of fractures during the rise of water) increases with depth. Thus, considering the profile view of the ridge, the 2D interpretation of the GPR data (figure 7) is consistent with the conclusion based on field observations. Although the current interpretation of the GPR data is theoretical, it is compatible with previous field observations (e.g., Altunel and Hancock 1996, Mesci 2004). However, confirmation of this would be obtained by either trial cores or an electromagnetic model and may be the subject of a subsequent paper.

Acknowledgments

I would like to thank Volkan Karabacak (Eskisehir Osmangazi University) for his help in the field. I am very grateful for the

helpful comments and constructive reviews by the anonymous referees, which improved my manuscript.

References

Altunel E 1994 Active tectonics and the evolution of Quaternary travertines at Pamukkale, Western Turkey *PhD Thesis* Bristol University p 236 unpublished

Altunel E and Hancock P L 1993a Morphology and structural setting of Quaternary travertines at Pamukkale, Turkey *Geol. J.* **28** 335–46

Altunel E and Hancock P L 1993b Active fissuring and faulting in Quaternary travertines at Pamukkale, Western Turkey. Neotectonics and active faulting *Z. Geomorphol. NF* **94** 285–302

Altunel E and Hancock P L 1996 Structural attributes of travertine-filled extensional fissures in the Pamukkale plateau, Western Turkey *Int. Geol. Rev.* **38** 768–77

Barnes I, Irwin W P and White D E 1978 *Global Distribution of Carbon Dioxide Discharges, and Major Zones of Seismicity* (Reston, VA: US Geological Survey Water Resources Investigations 78–39, Open-File Report)

Cakir Z 1999 Along-strike discontinuity of active normal faults and its influence on Quaternary travertine deposition; examples from Western Turkey *Turk. J. Earth Sci.* **8** 67–80

Carrozzo M T, Leucci G, Negri S and Nuzzo L 2003 GPR Survey to understand the stratigraphy of the Roman ships archaeological Site (Pisa, Italy) *Archaeol. Prospection* **10** 57–72

Cassidy N J 2009 Ground penetrating radar data processing, modelling and analysis *Ground Penetrating Radar: Theory and Applications* (Amsterdam: Elsevier) pp 141–76

Chafetz H S and Folk R L 1984 Travertines: depositional morphology and the bacterially constructed constituents *J. Sedim. Petrol.* **54** 289–316

Conyers L B 2004 *Ground-Penetrating Radar for Archaeology* (Walnut Creek, CA: Altamira Press)

Conyers L B 2006 Ground-penetrating radar techniques to discover and map historic graves *Historical Archaeol.* **40** 64–73

French W 1974 Two-dimensional and three dimensional migration of model-experiment reflection profiles *Geophysics* **39** 265–77

Hancock P L, Chalmers R M L, Altunel E and Çakır Z 1999 Travitonics: using travertine in active fault studies *J. Struct. Geol.* **21** 903–16

Jones J C 1925 *Travertine Company Report* UNR88-29 University of Nevada, Reno, USA (Special Collection) unpublished

Kadioglu S and Ulugergerli E U 2012 Imaging karstic cavities in transparent 3D volume of the GPR data set in Akkopru dam, Mugla, Turkey **27** 263–71

Leckebusch J 2003 Ground-penetrating radar: a modern three-dimensional prospection method *Archaeol. Prospection* **10** 213–40

Leckebusch J, Weibel A and Bühler F 2008 Semi-automatic feature extraction from GPR data *Near Surf. Geophys.* **6** 75–84

Leucci G and Negri S 2006 Use of ground penetrating radar to map subsurface archaeological features in an urban area *J. Archaeol. Sci.* **33** 502–12

Mesci B L 2004 The development of travertine occurrences around Sıcak Çermik (Sivas) and their relationships with active tectonics *PhD Thesis* Cumhuriyet University p 271 unpublished

Mesci B L, Gürsoy H and Tatar O 2008 The evolution of travertine masses in the Sivas area (central Turkey) and their relationships to active tectonics *Turk. J. Earth Sci.* **17** 219–40

Moran M L, Greenfield R J, Arcone S A and Delaney A J 2000 Multidimensional GPR array processing using Kirchhoff migration *J. Appl. Geophys.* **43** 281–95

Porsani J L, Sauck W A and Junior A O S 2006 GPR for mapping fractures and as a guide for the extraction of ornamental granite from a quarry: a case study from southern Brazil *J. Appl. Geophys.* **58** 177–87

Sandmeier K J 2003 Reflexw 4.2 Manuel Book: Sandmeier Software (Karlsruhe, Germany)

Saroglu F, Emre O and Kuscu I 1992 *Active Fault Map of Turkey* (Ankara: General Directorate of the Mineral Research and Exploration)

Schneider W A 1978 Integral formulation for migration in 2 and 3 dimensions *Geophysics* **43** 49–76

Sibson R H, Moore J M M and Rankin A H 1975 Seismic pumping a hydrothermal fluid transport mechanism *J. Geol. Soc. Lond.* **131** 653–9

Song J Y, Liu Q H, Torrione P and Collins L 2006 Two-dimensional and three-dimensional NUFFT migration method for landmine detection using ground-penetrating radar *IEEE Trans. Geosci. Remote Sens.* **44** 1462–9

Wyatt A 1986 *Challinor's Dictionary of Geology* 6th edn (Cardiff: University of Wales Press)

Yalçıner C Ç, Bano M, Kadıoglu M, Karabacak V, Meghraoui M and Altunel E 2009 New temple discovery at the archaeological site of Nysa (Western Turkey) using GPR method *J. Archaeol. Sci.* **36** 1680–9